



The level of iron enrichment required to initiate diatom blooms in HNLC waters

Mark L. Wells*

School of Marine Sciences, 5741 Libby Hall, University of Maine, Orono, ME 04469-5741, USA

Received 16 January 2002; received in revised form 20 March 2003; accepted 20 March 2003

Abstract

The chemical speciation of iron in seawater is controlled by complexation with organic ligands, the character of which likely regulates which phytoplankton groups can readily access this resource. Evidence from the IronEx II mesoscale iron enrichment experiment provides some insight to this regulation. Dissolved iron ($<0.4 \mu\text{m}$) in the enriched surface waters during IronEx II was partitioned into colloidal ($>1 \text{ kDa}$ – $0.4 \mu\text{m}$) and soluble ($<1 \text{ kDa}$) size fractions using cross flow filtration to better delineate iron dynamics with respect to phytoplankton growth. While dissolved concentrations in the patch increased by two orders of magnitude to $\sim 2 \text{ nM Fe}$, soluble concentrations only roughly doubled to $\sim 35 \text{ pM Fe}$, and this change occurred only during the first few days of the experiment. The subsequent decrease in soluble iron to ambient levels coincided with a dramatic increase in chlorophyll *a*, indicating that biological demand was responsible for the disappearance of soluble iron. This decrease also coincided with preferential drawdown of silicic acid over nitrate in the patch, indicating that diatoms were experiencing iron stress even as the bloom developed. Even so, calculations of the diffusional flux and iron uptake kinetics at the cellular level reveal that the concentrations of soluble iron during the later stages of the bloom were above that required to support continued rapid growth of the long, narrow pennate diatoms. This observation implies that the bulk of the organically bound soluble and colloidal iron was unavailable to meet the diatom growth requirements, and further that the measured increase in concentrations of strong Fe(III) complexing ligands impaired iron acquisition by diatoms. These findings indicate that excess macronutrients in HNLC waters might not be fully converted into diatom biomass even with repeated infusions of iron.

© 2003 Elsevier Science B.V. All rights reserved.

Keywords: Iron limitation; Phytoplankton; HNLC; Colloids; Cross-flow filtration

1. Introduction

The issue of iron limitation in the oceans continues to garner increasing interest, with mesoscale iron enrichment experiments now having been performed

in the equatorial Pacific (IronEx I, II), the Southern Ocean (SOIREE, SOFEX, EisenEx) and the Subarctic Pacific (SEEDS, SERIES). These experiments demonstrate that iron availability limits both diatom productivity and production in these persistently High Nitrate Low Chlorophyll (HNLC) regimes (Martin et al., 1994; Coale et al., 1996a; Boyd et al., 2000; Takeda et al., 2002; Cochlan, personal communication; Trick, personal communication). In each case,

* Tel.: +1-207-581-4322; fax: +1-207-581-4388.

E-mail address: mlwells@maine.edu (M.L. Wells).

iron infusions transformed the predominantly picoplanktonic phytoplankton assemblages into blooms of large diatoms, increasing total chlorophyll levels by an order of magnitude over that in the waters surrounding the enriched patches. The accompanying depletion of macronutrients and total CO₂ measured during the early stages of the IronEx II and SOIREE bloom experiments testify to the potential geochemical impacts that iron flux alone can have in these regions (Steinberg et al., 1998; Boyd et al., 2000). The enrichment experiments performed in the Southern Ocean (SOFEX, EisenEx) and the Subarctic Pacific (SEEDS, SERIES) had equally dramatic effects on the plankton assemblage. These findings have caused global climate change modelers to seek ways to incorporate iron into their models to account for natural (or anthropogenic) fluctuations in iron inputs to the oceans. However, critical questions remain unanswered about the cycling of iron speciation in seawater, its differential effects on iron availability to competing autotrophs, and thus its effects on ecosystem structure and carbon export.

The minimum change in iron inputs needed to initiate the transition from a largely recycling, picoplanktonic community to a nanoplanktonic, export-dominated ecosystem has not been determined. The maximum iron concentrations in the infused patches of IronExII (~ 2 nM) and SOIREE (~ 3 nM) (Coale et al., 1996a; Boyd et al., 2000) were small in comparison to coastal waters but represent a massive perturbation over the ambient dissolved iron concentrations at those sites (e.g., see in de Baar and de Jong, 2001), increasing iron levels by at least two orders of magnitude (Rue and Bruland, 1997; Boyd et al., 2000). Assessing the minimum iron enrichment needed to shift the ecosystem structure is important because it quantifies the scale of any natural perturbations that could initiate these bloom events. If a high iron flux, such as employed in all of the mesoscale iron enrichment studies to date, is required to trigger this transition, then iron-induced increases in export production could result only after climate change significantly altered atmospheric dust transport. However, if these ecosystem transitions can be initiated by very minor increases in iron flux, then iron-facilitated export production may help initiate and possibly accelerate global climate change (Martin, 1990; Sigman and Boyle, 2000).

Some insight into the minimum iron inputs needed to cause large diatom blooms in HNLC waters is gained by examining the partitioning of dissolved iron within the IronEx II patch between soluble and colloidal fractions. Although there remains considerable uncertainty about which iron species are available to phytoplankton in general, and to diatoms in particular, iron uptake appears to be restricted to the truly soluble, i.e., low molecular weight fraction in seawater (Wells et al., 1995; Sunda, 2001). Colloidal and particulate (>0.2–0.4 μm) iron forms can re-supply the reactive soluble species that are transported into the cell, but there is no physiological evidence that diatoms can directly move colloidal substances across their cell membranes (Rich and Morel, 1990; Sunda, 2001). If the colloidal re-supply rate to the soluble phase is too slow to match phytoplankton iron demand, then diatoms will experience iron stress despite an excess of total dissolved (colloidal + soluble) iron (Wells et al., 1983, 1991b). Similarly, iron may be complexed by organic chelators that reduce the ability of diatoms to extract soluble iron (Hutchins et al., 1999). Studying how soluble iron varies in conjunction with bloom evolution, and comparing this pool size to the apparent degree of iron stress experienced by phytoplankton, should provide some insight to how iron dynamics may affect phytoplankton growth and ecosystem structure.

Here I present results from cross-flow filtration (CFF) studies conducted during IronEx II where dissolved iron (<0.4 μm) was partitioned into colloidal (1 kDa–0.4 μm), and soluble (<1 kDa) size fractions. These results show that the high dissolved iron additions led to only marginal increases in soluble iron, with the bulk of added iron occurring in the colloidal phase. Soluble iron concentrations during IronEx II remained below the maximum inorganic solubility threshold (0.3 nM, see Liu and Millero, 2002), indicating that the size distribution of iron was regulated by organic complexation rather than precipitation of colloidal iron oxyhydroxides (Waite, 2001). But even with the presence of excess iron there are indications that the diatom population experienced iron stress during bloom development, suggesting that iron speciation became unfavorable for rapid diatom growth. These findings help to constrain the magnitude of iron flux needed to initiate and sustain large phytoplankton blooms in equatorial HNLC waters, and indicate that

total depletion of excess nitrate may not be attained even with prolonged increases in iron inputs.

2. Materials and methods

The IronEx II mesoscale iron-enrichment experiment was conducted 500 km southwest of the Galapagos Islands, starting at $\sim 4^{\circ}\text{S}$ 105°W . The results presented here are from the first of two iron infused patches where Fe(II)SO_4 in acidified seawater was pumped into the propeller wash while the ship followed a 8×9 km grid. The target concentration was 2 nM Fe within the 35-m surface mixed layer. An inert tracer (SF_6) was mixed with the iron stream to facilitate tracking of the patch, the center of which was marked by a drogue buoy. The patch was re-infused with iron on Day 3 and Day 7 of the experiment to maintain high dissolved iron concentrations. The resultant patch was tracked for 3 weeks as it drifted ~ 1200 km towards the southeast (Coale et al., 1996a).

Samples were collected from various locations near the center of the enriched patch using Teflon[®] lined 30 l GO-FLO bottles (General Oceanics) on a Kevlar line (Philadelphia Resins). M. Gordon (Moss Landing Marine Laboratory) kindly provided the conventionally filtered ($<0.4 \mu\text{m}$) samples for CFF processing. Water samples were filtered directly from the GO-FLO bottles using N_2 overpressure through acid-washed polycarbonate 142 mm diameter, $0.4 \mu\text{m}$ pore size Nuclepore filters mounted in Teflon (PTFE) filter sandwiches. These conventional filtrates were collected in 20 l fluorinated high density polyethylene carboys (Nalgene[®]) that had been rigorously acid cleaned. Samples were filtered in a trace metal clean van under a HEPA filtered air bench (Class 100). These steps have been demonstrated to provide uncontaminated samples for trace metal analysis (Bruland et al., 1979; Martin and Gordon, 1988).

The 20 l filtered ($0.4 \mu\text{m}$) carboy samples were transferred to a second clean van and were processed by CFF to partition metals into soluble and colloidal fractions. The CFF method continuously recirculated the sample under pressure across a filter membrane surface, so that on each pass a small fraction of the solution and solutes (the permeate) passed through the CFF membrane, leaving a slightly more concentrated colloidal fraction behind (retentate). Recirculation min-

imizes concentration polarization effects that result from accumulation of high solute and particle concentrations just above the membrane surface (Buffle et al., 1992). A silicone-encapsulated Filtron[®] polysulfone membrane (0.46 m^2) was sandwiched between polycarbonate leaves fitted with Teflon[®] tubing and connectors to enable sample recirculation and permeate collection. Continuous recirculation of the sample was done with a peristaltic pump (Masterflex) equipped with C-Flex (Cole Parmer) tubing.

The standardized operating protocol began with flushing the system with fresh sample, followed by recirculation of a fresh sub-sample for 10 min to precondition the membrane and system surfaces. This step minimizes the sorptive loss of iron and other constituents to the CFF system during the subsequent sample processing. The CFF system was then emptied and flushed again with fresh sample water before beginning sample processing. Retentate recirculation rates were $\sim 4 \text{ l min}^{-1}$ at a total system pressure of 140 kPa, and permeate flow rates were 80–90 ml min^{-1} . The transmembrane pressure (that is, the pressure loss due to filtration) was maintained at <70 kPa by adjusting Teflon[®] backpressure valves on the permeate (<1 kDa) and retentate (>1 kDa) return lines. Final concentration factors were kept below six because the chance of colloid breakthrough may increase with high concentration factor (Buessler et al., 1996; but also see Guo et al., 2000; Wells, 2002). To test for breakthrough artifacts, permeate samples were collected at the start and end of CFF processing. When ~ 2.5 l of sample retentate remained, the permeate valve was closed, the backpressure valve opened fully, and the retentate fraction recirculated freely for 10 min before halting the process and collecting the retentate sample. This extra step helps minimize colloid loss within the system (see Buessler et al., 1996). CFF processing was completed within ~ 5 h of sample collection. Samples were acidified with 4 ml of quartz-distilled 6 N HCl/l and stored for several months before extraction and analysis. Between samples, the membranes and CFF system were cleaned by recirculating 25% methanol (Fisher Optima) in 10% HCl (TM grade) for 15 min and rinsed thoroughly with deionized water. The membranes then were stored in 10% HCl (TM grade) until the next sampling period.

After several months of acidification, iron was extracted from the dissolved ($<0.4 \mu\text{m}$), permeate

(<1 kDa) and retentate (1 kDa–0.4 μm) samples by solid phase extraction (Wells and Bruland, 1998). Briefly, the metal complexing ligand hydroxy-diethyl-dithiocarbamate was added to 500 ml acidified samples and the pH adjusted to 8 with buffer and Q-NH₄OH (Q=quartz distilled). Samples were pumped through a polystyrene-based C-18 resin that retained the metal ligand complexes. Columns were eluted with 1 N Q-HNO₃ in Q-methanol into 3 ml Teflon vials and the extracts taken to dryness and re-constituted with 2 ml of 0.1 N Q-HNO₃. The method blanks (column + reagent) were determined by processing deionized water containing equivalent concentrations of buffer and ligand immediately prior to the samples.

The sample extracts were analyzed on a Finnigan MAT ELEMENT magnetic sector (high resolution) ICP-MS. Extracts were pumped into a CETAC[®] microconcentric nebulizer (MCN-100) at a flow rate of 60 $\mu\text{l min}^{-1}$ while the ICP-MS scanned the mass concentrations of the dominant natural isotope of iron ($\text{amu}=56$). The sample peak was scanned for 0.01 s and the run repeated 20 times. Concentrations were determined by comparison to linear standard curves generated from analysis of standards prepared in 0.1 N HNO₃. The sample concentrations reported here are the mean of these 20 measurements, normalized to an internal standard (20 ppb In) in the 0.1 N HNO₃ used to reconstitute the evaporated column extracts. This internal standard, measured on each run, corrects for minor changes in instrument sensitivity during analyses. The high instrument sensitivity (>10 Mhz/ppm In

(115) at a resolution of 4000) and low background (dark noise <0.2 counts/s) combined with the low method blank (see details in Wells and Bruland, 1998) and large sample volume extracted (500 ml) yielded an analytical detection limit of 9 pM Fe ($3 \times$ S.D. of 12 blank analyses).

Colloid concentrations were calculated from the concentration factor (cf) of the individual CFF run and the measured metal concentrations in the retentate and permeate fractions, i.e.,

$$[\text{colloid}] = \frac{[\text{retentate}] - [\text{permeate}]}{\text{cf}}$$

This quantification of colloid concentrations is more robust than simply subtracting permeate (<1 kDa) from total dissolved (<0.2 μm) concentrations because the latter depends on accurately measuring the difference between two large numbers, and because the mass balance can be determined for each CFF run, i.e.,

$$[< 0.2 \mu\text{m}] = [\text{permeate}] + [\text{colloid}]$$

In this way, a good agreement between the sum of permeate and calculated colloid concentrations with dissolved values suggests that CFF processing was not affected significantly by contamination or sorptive losses to the membrane.

These precautions notwithstanding, it is important to recognize the arbitrary nature of size cutoff with CFF techniques, and that CFF membranes are fabri-

Table 1
CFF iron data from Patch 1 during IronEx II

Day	<1 kDa #1 (pM)	<1 kDa #2 (pM)	>1 kDa (pM)	<0.4 μm (pM)	% Mass balance	Colloidal Fe (pM)
–1	19 \pm 1	13 \pm 0.5	152 \pm 22	22 \pm 0.5	104	3.0
1.0	34 \pm 8	30 \pm 2	1200 \pm 50	1350 \pm 250	22	1318
1.8	41 \pm 8	31 \pm 4	683 \pm 16	230 \pm 32	90	190
3.4	42 \pm 5	12 \pm 1	572 \pm 28	425 \pm 91	26	398
5.1	21 \pm 1	49	284 \pm 69	115 \pm 15	95	94
6.2	15	[51]	176 \pm 11	36 \pm 1	90	21
8.2	22 \pm 2	21	–	56 \pm 9		33
9.0	14 \pm 1	27 \pm 1	166 \pm 15	32 \pm 1	96	18

Values for the <1 kDa samples collected at the beginning (#1) and end (#2) of CFF processing are shown. The >1 kDa values are the raw concentrations measured in this fraction. Colloidal iron values were calculated as $([\text{retentate}] - [\text{permeate}])/\text{cf}$ (see Materials and methods). The mean and range of duplicate analyses for each sample are shown where available. The missing iron indicated by the low CFF recovery on days 1 and 3.4 was added to the colloid fraction (see text). The bracketed value on day 6.2 is suspect due to a CFF processing error and is not included in Fig. 1.

cated for mainly industrial purposes rather than as accurate or precise size separation devices. Moreover, there remain significant questions about how operational protocols may influence the behavior of natural colloidal matter in these systems (e.g., see Dai et al., 1998; Guo et al., 2000). Nonetheless, CFF remains an extremely useful tool for assessing the broad characteristics and abundance of the marine colloidal phase, and the uniform application of CFF in this study allows the assessment of temporal trends in colloid and soluble partitioning of iron.

3. Results

Iron concentrations in the dissolved, permeate and retentate size fractions are given in Table 1 along with the colloidal concentrations and mass balances calculated for the separations. Good mass balance was achieved for all samples (90–105%) except for those obtained immediately after the first and second iron infusions to the patch, when recoveries were 22% and 26%, respectively. These poor iron recoveries are attributed here to retention of surface active colloidal iron oxyhydroxides on the filter membranes rather than the sorption of soluble iron species (see Discussion).

Samples taken before the iron infusion indicate that ~ 85% of the ambient dissolved iron (22 pM) was soluble in nature and the remaining ~ 15% (3 pM) occurred in the colloidal phase (see Materials and methods). Reliable determinations of such small colloidal concentrations within the dissolved phase would be impossible from the simple difference between dissolved (<0.4 μm) and permeate (<1 kDa) values. However, in this case the comparatively high iron concentration in the colloidal retentate (152 ± 22 pM Fe) and the good mass balance for this separation (104%) indicates that this soluble/colloidal partitioning was reasonably accurate.

Dissolved iron concentrations within the enriched patch cycled repeatedly from nanomolar to picomolar levels, decreasing sharply after each infusion (Fig. 1A). The rate that iron disappeared progressively increased from the first to third infusions. The vast majority of the added iron was found in the colloidal phase, with soluble (<1 kDa) concentrations increasing by only ~ 25 pM over ambient levels (Fig. 1B,C). The percentage of colloidal iron decreased from near

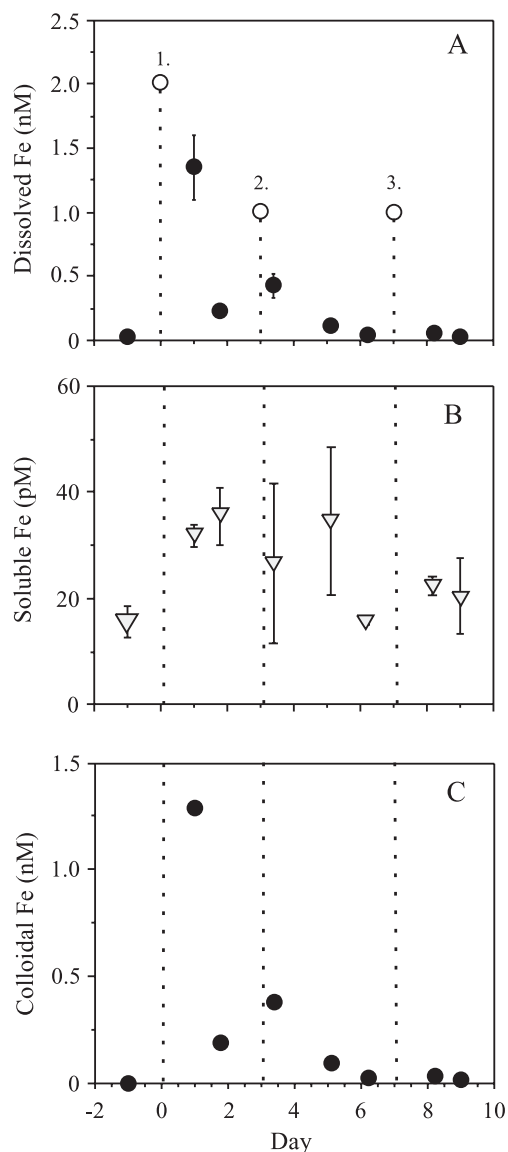


Fig. 1. Concentrations of (A) dissolved (<0.4 μm), (B) soluble (<1 kDa), and (C) colloidal (>1 kDa–0.4 μm) iron measured during IronEx II. Open circles indicate target iron concentrations within the patch upon each of three infusions. Bars indicate the range between duplicate analyses when larger than the symbol size.

100% immediately following the first infusion to ~ 60% nine days later (Fig. 2A). Colloidal sized phases continued to dominate iron speciation even when total dissolved iron concentrations fell to near pre-release levels within the patch (Figs. 1A and 2A). The insensitivity of soluble iron concentrations to

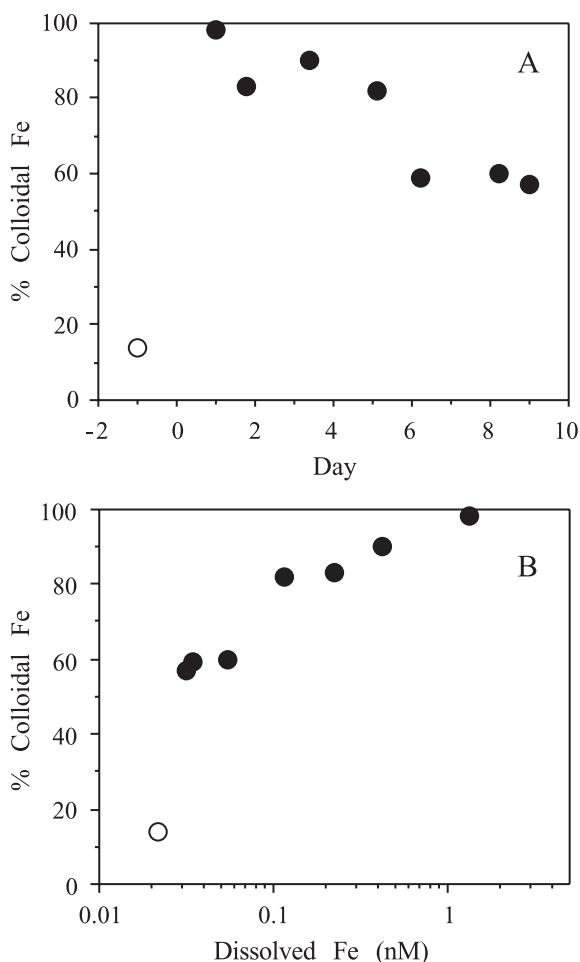


Fig. 2. (A) The percent of colloidal iron in the dissolved fraction as a function of time after infusion, and (B) as a function of the total dissolved iron concentration.

changes in total dissolved ($<0.4 \mu\text{m}$) iron is illustrated in Fig. 2B, where the percent colloidal iron fell by only a factor of 2 compared to almost two orders of magnitude decrease in dissolved iron concentrations.

Soluble iron concentrations increased roughly two-fold from 16 to $\sim 35 \text{ pM}$ Fe over the 4 days following the first infusion (Fig. 1B). This increase in soluble iron preceded the start of chl *a* buildup by 2 days (Fig. 3). After chl biomass (and thus carbon biomass; see Landry et al., 2000) began to increase dramatically on Days 5–6, soluble iron concentrations dropped sharply and then remained at near pre-release levels through Day 9, the final day of CFF sampling.

Bloom development led to a rapid drawdown of nitrate and silicic acid (Fig. 4A), although as the bloom developed their relative consumption changed significantly. The $\text{Si(OH)}_4/\text{NO}_3$ concentration ratio in surface waters was ~ 0.5 at the start of the experiment, the relative depletion of silicic acid being indicative of an iron-limited system (Hutchins and Bruland, 1998; Takeda, 1998). The nutrient consumption ratio ($\Delta\text{Si(OH)}_4/\Delta\text{NO}_3$) during the early stage of bloom development (Day -1 to 4.5) was ~ 0.6 (determined as the ratio of negative slopes of concentrations vs. time). Thus there was a slight preferential uptake of NO_3 over Si(OH)_4 as the ecosystem began to respond. However, the sign of this consumption ratio reversed (Si(OH)_4 uptake became $>\text{NO}_3$ uptake) and the value increased to ~ 2 between Days 5 and 10. This change is illustrated clearly by the decrease in $\text{Si(OH)}_4/\text{NO}_3$ concentration ratios after the second iron infusion on Day 5 (Fig. 4A,B), roughly half way towards the bloom maximum (Fig. 4A,B). The subsequent linear decrease in dissolved $\text{Si(OH)}_4/\text{NO}_3$ ratios after Day 5 were synchronous with the decrease in soluble iron concentration (Fig. 4B,C). The minimum dissolved $\text{Si(OH)}_4/\text{NO}_3$ concentration ratio of 0.14 occurred on Day 13 after chl *a* concentrations peaked and the ratio began to increase again in conjunction with decreasing in chl *a* concentrations (Fig. 4B).

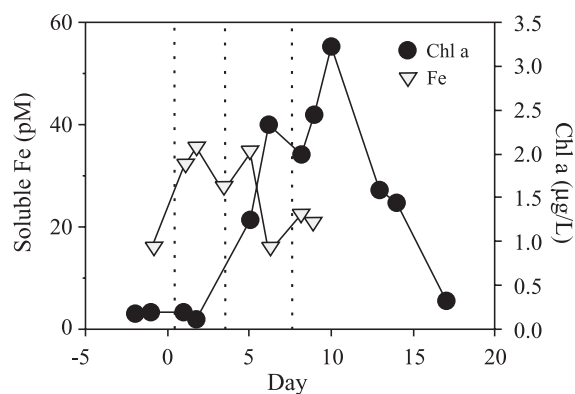


Fig. 3. The change in soluble ($<1 \text{ kDa}$) iron concentrations within the patch in relation to average chl *a* concentrations in the upper mixed layer (data kindly provided by K. Coale, MLML). Error bars for chl *a* depict ± 1 S.D.; range bars for the soluble iron concentrations are omitted here for clarity (see Fig. 1B).

4. Discussion

The strength of these findings strongly depends on both the accuracy of iron determinations and the effectiveness of partitioning the dissolved iron into soluble and colloidal fractions at these very low (nanomolar to picomolar) concentrations. The solid phase extraction method used here has been verified against the traditional solvent extraction method (Bruland et al., 1979). In this case, the high preconcentration factors used and precision of replicate extractions with the solid phase method, combined with the detection sensitivity of high-resolution ICP-MS, yield an extremely low (~ 9 pM) analytical detection limit for iron (Wells and Bruland, 1998). These dissolved iron measurements correspond well with independent voltammetric determinations by Rue and Bruland (1997) on samples drawn at similar time points, although small differences were found on occasion. For example, the dissolved concentrations reported here near the peak of the bloom (Day 9) were higher than measured by Rue and Bruland (32 pM vs. 13 pM). This discrepancy might be ascribed to the prolonged acidification of the samples here (= 6 months) compared to the short-term UV irradiation method used by Rue and Bruland (e.g., see Bruland et al., 2001). However, these measurements also were not determined from samples taken on the same bottle cast, so it is more likely that the difference results from small variations in iron distribution within the patch.

The mass balances for CFF processing were better than 90% in all but two cases, providing a high degree of confidence in these size separations. The two cases where mass balances were substantially lower ($\sim 25\%$) occurred with samples collected immediately after the first and second iron infusions. In theory, these lower recoveries could be due to the sorption of soluble inorganic Fe(III) species or organic Fe(III) complexes to the membrane or to adhesion of colloidal (organic or inorganic) iron. The excellent mass balances obtained at other time points, when organic complexation dominated the chemical speciation of Fe(III), suggests that sorption of soluble or colloidal organic Fe(III) forms was minimal. The chemical speciation of Fe(III) was almost completely dominated by organic complexation from the start (Rue and Bruland, 1997), so sorption of soluble inorganic Fe(III) species was unlikely to be signifi-

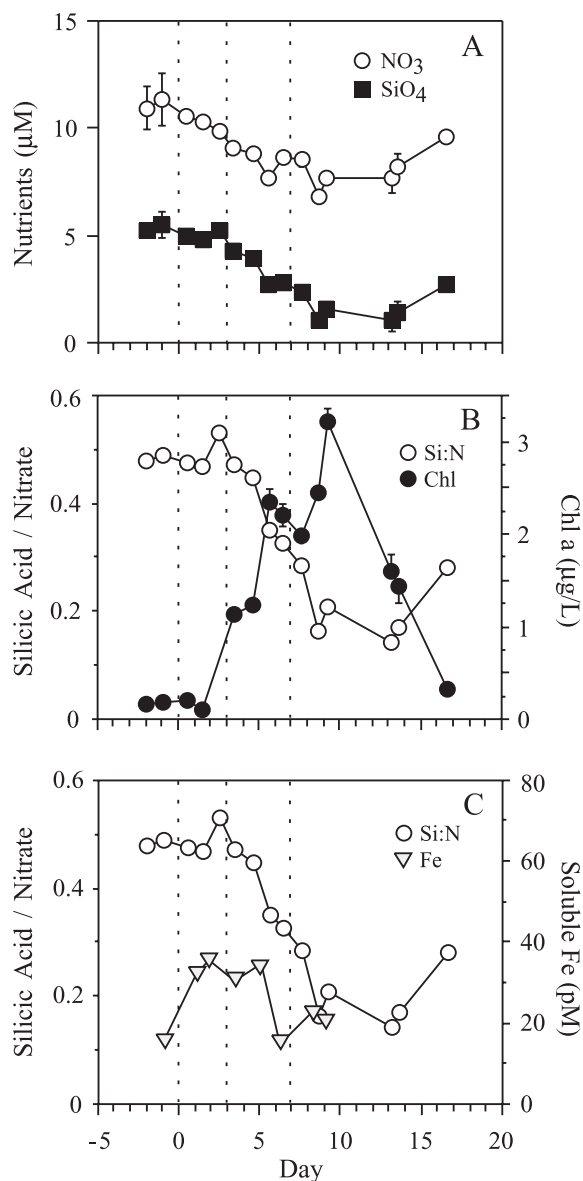


Fig. 4. (A) The decrease in nitrate (open circles) and silicic acid (filled squares) during the course of the bloom (data kindly provided by K. Coale, MLML). (B) The change in the ratio of dissolved silicic acid to nitrate (open circles) during development of the bloom in relation to surface averaged chl *a* concentrations (filled circles). A marked shift in draw down ratios is observed after Day 4. (C) Changes in soluble iron concentrations in relation to the shift in silicic acid/nitrate draw down ratios.

cant. The same would not be true for colloidal Fe(III) oxyhydroxides. The infused Fe(II) would have been largely oxidized to Fe(III) within ~ 30 min under the release conditions (Millero and Sotolongo, 1989; Johnson et al., 1994; Moffett, 2001), yielding very high (≥ 40 nM) Fe(III) concentrations within the partially dispersed plume (K. Johnson, personal communication). Colloidal Fe(III) oxyhydroxides would precipitate rapidly under these conditions and the resultant surface active amorphous colloids are the most likely cause for the poor recoveries obtained immediately following the infusions. Although photolysis would have influenced iron redox chemistry within the enriched patch (Wells et al., 1991a; Johnson et al., 1994; Barbeau et al., 2001; Moffett, 2001), there is no evidence that Fe(II) species comprised a significant fraction of the iron pool (Rue and Bruland, 1997). This situation apparently differs from the SOIREE experiment where Fe(II) appeared to comprise the major portion of dissolved Fe species (Croot et al., 2001), perhaps due to temperature effects on the rates of Fe(II) oxidation (Boyd et al., 2000).

The pre-release sample contained $\sim 15\%$ colloidal iron within the 20 pM ambient dissolved Fe phase, as defined by the CFF method used here. This percentage is substantially lower than reported for the North Atlantic and North Pacific (80–90%; Wu et al., 2001) but is more similar to some results from eastern Subarctic Pacific HNLC waters (Nishioka et al., 2001). Boyé et al. (2002) found that colloidal iron >200 kDa in size accounts for a major fraction of dissolved iron in Southern Ocean waters. The differences in methodologies used among these three studies makes quantitative comparisons highly suspect (see Wells, 2002). Even so, the low percent colloidal value here may well reflect the extremely low dissolved concentration of iron compared to that more typical of the sub-tropical gyres off Hawaii and Bermuda (Wu et al., 2001). For example, the percent colloidal Fe fraction measured in nearshore waters often is $\gg 50\%$ (Whitehouse et al., 1990; Benoit et al., 1994; Dai and Martin, 1995; Martin et al., 1995; Powell et al., 1996; Sanudo-Wilhelmy et al., 1996; Guieu et al., 1998; Wen et al., 1999; Gustafsson et al., 2000; Wells et al., 2000).

The findings here demonstrate that the vast bulk of the iron within the enriched patch, whatever its form or chemical speciation, was colloidal and not truly

soluble. This colloidal sol was largely unstable under these conditions, leading to the rapid loss of iron from the dissolved phase (Fig. 1). The colloidal proportion of the infused iron appeared to decrease progressively after each enrichment, from 99% to 90% and then to 60% of the nominally “dissolved” iron (Fig. 2A). This decrease was not due to a repartitioning of iron into the soluble phase, but rather to the decrease in total dissolved iron concentrations (Figs. 1A and 2B). It is anticipated that inorganic colloidal Fe(III) oxyhydroxides would aggregate rapidly (e.g., Honeyman and Santschi, 1989), and this removal mechanism is consistent with the kinetics of infused iron loss measured in equatorial surface waters (Gordon et al., 1998). It additionally is possible that colloidal iron removal was facilitated with the scavenging of macrogels formed at the time of iron infusion (see Chin et al., 1998).

It is noteworthy that in contrast to the later SOIREE experiment in the Southern Ocean (Boyd et al., 2000), dissolved iron concentrations (colloidal plus soluble) during IronEx II did not remain elevated after the final enrichment but in fact decreased near the end of the bloom to below the pre-release concentrations (Rue and Bruland, 1997). This disappearance of dissolved iron occurred even with elevated concentrations of organic ligands being present (Rue and Bruland, 1997) and presumably results from the combined effect of colloidal iron aggregation and high iron demand of the diatom population.

So how would the changes in abundance of soluble and colloidal iron affect the biological response? Addressing this question is difficult because the answer depends strongly on how diatoms acquire iron to meet their growth requirements; a major question facing marine biogeochemists today. While it has been shown that one marine mixotroph acquires iron by ingesting other organisms (Maranger et al., 1998), there is broad consensus that diatoms can only sequester Fe(III) species from the soluble (or low molecular weight) phase (Wells et al., 1983, 1995; Rich and Morel, 1990; Hutchins et al., 1999; Sunda, 2001). Accepting the alternate hypothesis requires clear evidence that diatoms can transport colloidal-sized (>1 kDa) substances across their cell membranes; a feature that at least prokaryotic organisms appear to be unable to accomplish (Payne, 1980). Although not all soluble Fe(III) species may be

available for uptake (Hutchins et al., 1999), the iron supply to diatoms nonetheless should arrive through the soluble fraction. Changes in soluble iron concentrations over the course of the bloom should then reflect the balance between iron supply and the biological demand.

Soluble iron concentrations roughly doubled after the initial iron infusion, from ~ 16 to ~ 35 pM, and then remained elevated over the next 4 days (Table 1, Fig. 1B). But soluble concentrations did not increase further after infusions on Day 3 or Day 7 of the experiment. Rue and Bruland (1997) found that the concentrations of organic Fe(III) complexing ligands increased by 400% during this period to ~ 2 nM, with most of the increase attributed to the stronger ligand class. The results here indicate that the bulk of the Fe(III)–ligand complexes at this time point were colloidal in size, in contrast to the pre-release conditions, where the strong Fe(III)–ligand complexes were mainly soluble (Table 1, Fig. 1C). This apparent increase in ligand size may indicate that iron infusion triggered release of ligands having markedly different (i.e., larger) molecular architectures (but equivalent binding constants for Fe(III)). Indeed, a small portion of the ligands in the pre-release samples also were large; roughly 15% of dissolved iron (bound by strong Fe(III) complexing ligands; Rue and Bruland, 1997) was retained by the 1 kDa membrane (Table 1, Fig. 2A). The iron infusion perhaps caused some organisms to release a different type of ligand, or perhaps there was a change in the main source of Fe(III) complexing ligands. A speculative alternative is that the rapid biological response to iron enrichment (Behrenfeld et al., 1996; Cavender-Barnes et al., 1999) increased the production of colloidal polymer matrices (Chin et al., 1998) to which low molecular weight Fe(III) complexing ligands became associated. In any event, the findings show that the majority of infused iron was not soluble and thus likely was not directly accessible to the rapidly dividing diatom cells.

The sharply increasing iron demand by the diatom population is indicated by the rapid depletion of soluble iron after Day 5, in conjunction with increasing chl *a* concentrations (Fig. 3). This depletion in soluble iron was almost certainly insufficient to support the observed bloom development. Chlorophyll *a* concentrations increased by $\sim 3 \mu\text{g l}^{-1}$ over the first 9 days, corresponding to an estimated net carbon fixation of

$\sim 1.9 \times 10^{-5} \text{ mol C l}^{-1}$ (based on a value of 0.18 mM chl *a*/mole diatom C measured during the bloom; Landry et al., 2000). The smallest known iron quota for an oceanic diatom is $\sim 5 \mu\text{mol Fe/mol C}$ (Sunda and Huntsman, 1995), indicating that the minimum amount of iron needed to fuel this increase in diatom population would have been ~ 95 pM. This calculation probably underestimates the actual iron demand because grazing pressure (Fe loss) is not taken into account (Bollens and Landry, 2000), and because large oceanic diatoms may have higher cellular iron quotas (Timmermans et al., 2001). Based then upon our current understanding of how diatoms acquire iron, a significant iron flux from colloidal to soluble iron species was required to support the rapid diatom growth observed.

The maximum estimated diatom growth rates during the initial stage of the bloom (1.6 – 1.9 day^{-1} ; Landry et al., 2000) are close to estimates for the temperature dependent maximum (1.9 day^{-1} ; Eppley, 1972). Even so, there is evidence that the diatoms did not fully escape iron limitation. Diatoms did not produce the electron transport protein ferrodoxin (Erddner and Anderson, 1999) suggesting that the metabolic iron demand was not entirely satisfied, and indeed photosynthetic efficiency declined very shortly after the last iron addition (Behrenfeld et al., 1996). Also, the significant increase in silicate uptake relative to nitrate by Day 6 of the experiment (Fig. 4B), roughly mid way through bloom development, is symptomatic of iron-stressed cells (Hutchins and Bruland, 1998; Takeda, 1998). These three independent indicators suggest then that diatoms were experiencing iron stress well before the bloom maximum, and that the final iron enrichment on Day 7 did little to alleviate this stress. As a consequence, the geochemical impact of the diatom bloom with respect to the drawdown of nitrate and total CO_2 (Steinberg et al., 1998) was smaller than it otherwise would have been had the utilization of silicic acid been more efficient.

In theory, this iron stress can be ascribed to one of two reasons. First, available iron concentrations may have decreased below the diffusion-limited threshold for rapid diatom growth and second, the iron flux to this available pool may have been insufficient to meet the diatom requirements. While these two factors can be linked (e.g., available iron is drawn below the diffusion-limited threshold concentration due to insuf-

ficient flux from the colloidal phase), they also may act independently (e.g., available soluble iron concentrations are maintained below the diffusion-limited threshold by organic complexation regardless of the flux from the colloidal phase). The balance between these limiting factors likely would have been affected by the increasing iron demand as the bloom developed; that is, higher cell numbers and possibly increasing cellular iron quotas due to potential self-shading effects at high biomass (Sunda and Huntsman, 1998). Changes in the character of Fe(III) complexing ligands initiated before the bloom fully developed could have worked against the increasing iron demand by decreasing the concentrations of accessible iron species.

Ascertaining the specific cause(s) for the iron stress that appeared to occur during IronEx II (data herein), SOIREE (Boyd et al., 2000) and SEEDS (Takeda et al., 2002) is important because it will help to constrain the magnitude of natural perturbations required to generate intense diatom blooms in HNLC waters. This understanding, in turn, would provide some insight to the scale of climatological factors needed to significantly affect carbon cycling in these waters. For example, if multiple iron additions each yielding >1 nM Fe could not provide the flux needed to support unrestrained diatom growth, then massive and persistent dust deposition (that is, significant global climate change) would be needed *before* diatom blooms might consume all of the excess macronutrients. However, if the diatom population instead became iron limited because increasing ligand concentrations drove available iron species below the diffusion-limited threshold for optimal growth, then even prolonged increases in atmospheric iron inputs to HNLC waters might never lead to an iron-induced elimination of excess macronutrients in these regions.

What proportion of the soluble iron measured during IronEx II would have to be available to support the observed diatom growth? This question can be approached using cell uptake analysis. The diffusion limited threshold for iron uptake is a function of growth rate (μ), cellular iron quota (Q), and net diffusion rate (k_D) of soluble species to the cell surface (Hudson and Morel, 1993). Assuming that diatoms are capable of acquiring $\sim 75\%$ of iron diffusing to the cell surface, the iron concentration needed to

support their growth can be expressed as (Hudson and Morel, 1993):

$$\mu Q = \frac{3}{4} k_D [\text{Fe}_{\text{avail}}] \text{ or } [\text{Fe}_{\text{avail}}] = \frac{4\mu Q}{3k_D}$$

Iron diffusion to the cell (k_D) in turn is a function of cell size and shape (Gavis, 1976),

$$k_D = 4\pi\alpha RD$$

where R is the cell radius along the major axis, D is diffusivity of the chemical species, and α is a shape factor for the cell ($\alpha=1$ for sphere). Initial stages of the IronEx II bloom were dominated by diatoms that were $\sim 24 \times 1.2 \mu\text{m}$ in size but cell sizes increased later in the bloom to $70 \times 3.5 \mu\text{m}$ (S. Tanner, MLML, personal communication). For diatoms idealized as prolate spheroids, the shape factor can be approximated as:

$$\alpha \cong 2 \frac{e}{\ln[(1+e)/(1-e)]} \text{ and } e = \sqrt{1 - a^2/R^2}$$

Where a is the semi-minor axis and R is the semi-major axis of the ellipsoid (Gavis, 1976). This numerical approach for estimating the iron needed for growth is considerably more simplistic than the uptake model given by Völker and Wolf-Gladrow (1999), but its advantage here is that fewer assumptions are needed regarding iron speciation, uptake mechanisms, and the rate constants appropriate for oceanic diatoms.

Using this analysis approach the iron requirements for pennate and centric diatoms are compared as a function of cell length (Fig. 5). By this estimate, pennate diatoms 24 μm in length would require steady state available iron concentrations of only $\sim 0.3 \text{ pM}$ Fe while the larger cells that appeared later in the bloom ($\sim 70 \mu\text{m}$ in length) could maintain rapid growth at a steady state concentrations of $\sim 2.5 \text{ pM}$ available Fe. A similar threshold concentration ($\sim 2 \text{ pM}$) is calculated independently based on the Michaelis–Menten rate law (Appendix A). These values are in the range determined by Timmermans et al. (2001) for pennate diatoms isolated from Southern Ocean waters. By comparison, centric diatoms 15 μm in diameter require 160 times greater steady state soluble iron concentrations in order to escape diffusion limitation. While there is a clear inverse relationship

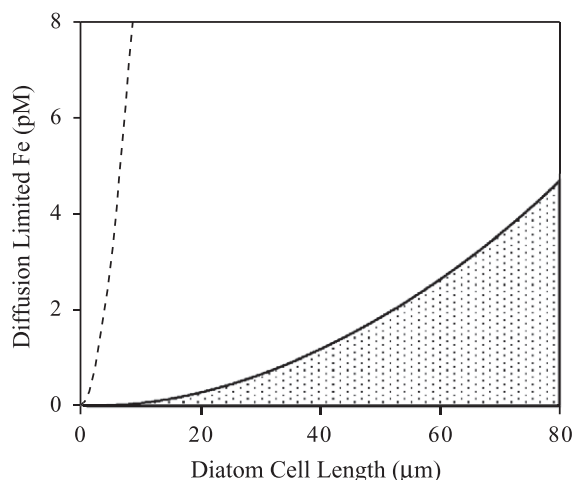


Fig. 5. Estimated available iron concentrations required for diffusion-limited growth of diatoms as a function of cell length. The solid line depicts the steady state iron concentration where diffusion rate to the pennate diatom cell matches the cellular requirements for a growth rate of 1 day^{-1} . Shaded area indicates iron deficient conditions. Dashed line represents the requirement if the cell had a centric shape of equivalent length. The parameters chosen for this calculation were a molecular diffusivity of $0.9 \times 10^{-5} \text{ cm}^2 \text{ s}^{-1}$ (i.e., Fe(III) species sized near inorganic complexes), a cellular iron content of $50 \mu\text{mol l}^{-1}$ of cytoplasm (Sunda and Huntsman, 1995), and a cellular aspect ratio of 20 (length/width).

between cell size and iron uptake rates for idealized cells (Sunda, 2001), the calculations here illustrate the important effect of cell shape. Even large ($>20 \mu\text{m}$ in length) pennate diatoms can enjoy a substantial benefit over their centric counterparts under low iron conditions, which may help explain why pennate diatoms tend to dominate after most of the mesoscale iron enrichments to date (e.g., see in Landry et al., 2000). It perhaps is not surprising then that the periodic paleodiatom blooms recorded in eastern Equatorial Pacific sediments over the last 18 million years comprise mainly pennate diatoms (Kemp and Baldauf, 1993). Observations of iron-initiated centric diatom blooms in the western Subarctic Pacific (SEEDS) and in the Pacific sector of the Southern Ocean (SOFEX) raise important questions about how uniform iron limitation is among HNLC regions, and what other chemical or physical factors might enhance the growth of centric over pennate diatoms.

The calculated threshold concentrations for rapid growth of centric and pennate diatoms lie an order of

magnitude below the measured soluble concentrations of iron during IronEx II (Table 1, Rue and Bruland, 1997). This finding implies that the majority of the ambient organic-iron complexes were unavailable for rapid uptake by diatoms. Moreover, this condition apparently was not reversed by the iron infusion on Day 7 (Fig. 4B,C), implying that the iron stress of diatoms was not attributable to a restrained iron flux from the colloidal phase to soluble, available iron species. Hutchins et al. (1999) reported that diatoms were unable to readily access iron bound by presumed analogs of the strong ligand class in seawater and the results here provide indirect support to this finding. One implication from these findings is that the excess macronutrients in HNLC waters may not become fully converted into diatom biomass even after repeated or prolonged infusions of iron. This suggestion differs from results of bottle enrichment studies where complete nutrient drawdown is observed (e.g., Martin and Fitzwater, 1988). It is not yet clear why bottle experiments consistently differ in this way, but it may be partly because iron is not lost from the closed bottle system (that is, no sinking Fe(III) aggregates) or possibly because UV A induced photochemical cycling of iron is enhanced in the on-deck experiments relative to in-situ conditions (Wells et al., 1991a; Johnson et al., 1994; Barbeau et al., 2001; Moffett, 2001).

The results of this study suggest that soluble iron concentrations need only increase slightly ($\leq 25 \text{ pM}$) above ambient levels for large diatoms to grow rapidly. It is likely then that very small but continuous increases in iron flux might still stimulate large diatom blooms in HNLC waters. Moreover, if picomolar level iron perturbations do not trigger the enhanced release of strong iron-complexing ligands, smaller continuous iron enhancements might increase the efficiency of the diatom response. While speculative, a greater geochemical impact from subtle (rather than larger) iron perturbations might help explain why very intense pennate diatom paleodeposition events in the eastern equatorial Pacific frequently appear to have occurred independently of large-scale climate change (e.g. Piasias et al., 1995; Wells et al., 1999). However, HNLC ecosystem responses may become muted with respect to diatom growth if increased concentrations of strong Fe(III)-complexing organic ligands appear and persist. A reappearance of iron stress in the

middle of bloom development also was seen during SOIREE (Boyd et al., 2000; Maldonado et al., 2001), suggesting that this phenomenon may be a characteristic outcome of large, pulsed inputs of iron. Studies of the longer-term ecosystem responses to prolonged iron perturbations, and in particular the influence of changing ligand abundance, are needed before we can better assess not only how iron is linked to biological and geochemical signals recorded in marine sediments, but also to determine its past effects on the drawdown on atmospheric carbon dioxide.

Acknowledgements

I wish to express my appreciation to K. Coale and K. Johnson for their excellent cruise support and my particular thanks to M. Gordon for kindly providing the sample filtrates used for all of the cross flow separations reported here. I also wish to thank H. de Baar and three anonymous reviewers for their helpful suggestions and comments that greatly improved an earlier version of this manuscript. This work was supported by ONR grant N00014-93-1-0039 and NSF OCE-9617719.

Associate editor: Dr. Hein de Baar.

Appendix A

Michaelis-Menten (1913) kinetics can be used to estimate the minimum steady-state iron concentration needed to sustain maximal diatom growth. The cellular iron quota (U_{Fe}) can be calculated as

$$U_{\text{Fe}} = \frac{V_{\text{max}}(\text{Fe})[\text{Fe}_{\text{avail}}]}{K_{\text{m}}(\text{Fe}) + [\text{Fe}_{\text{avail}}]} \text{ which reduces to}$$

$$U_{\text{Fe}} = \frac{V_{\text{max}}(\text{Fe})}{K_{\text{m}}(\text{Fe})} [\text{Fe}_{\text{avail}}]$$

at low substrate concentrations. $V_{\text{max}}(\text{Fe})$ is the saturated iron uptake rate and $K_{\text{m}}(\text{Fe})$ is the half-saturation constant for iron, having the dimension of a concentration. An upper limit of the measured value for $V_{\text{max}}(\text{Fe})$ is $2700 \mu\text{mol Fe (l cell volume)}^{-1} \text{ day}^{-1}$ (Sunda and Huntsman, 1995) and a half-saturation constant of 0.12 nM has been measured in equatorial Pacific waters (Coale et al., 1996b). For a minimum

cellular iron content of $50 \mu\text{mol l}^{-1}$ of cytoplasm (Sunda and Huntsman, 1995) and a pennate diatom with an aspect ratio of 20 (length/width), a steady state iron concentration of $\sim 2 \text{ pM Fe}$ is needed to support pennate diatoms $70 \mu\text{m}$ in length growing at 1 day^{-1} .

References

- Barbeau, K., Rue, E.L., Bruland, K.W., Butler, A., 2001. Photochemical cycling of iron in the surface ocean mediated by microbial iron(III)-binding ligands. *Nature* 413 (6854), 409–413.
- Behrenfeld, M.J., Bale, A.J., Kolber, Z.S., Aiken, J., Falkowski, P.G., 1996. Confirmation of iron limitation of phytoplankton photosynthesis in the equatorial Pacific Ocean. *Nature* 383, 508–511.
- Benoit, G., et al., 1994. Partitioning of Cu, Pb, Ag, Zn, Fe, Al, and Mn between filter-retained particles, colloids and solution in six Texas estuaries. *Marine Chemistry* 45, 307–336.
- Bollens, G.C.R., Landry, M.R., 2000. Biological response to iron fertilization in the eastern equatorial Pacific (IronEx II). II. Mesozooplankton abundance, biomass, depth distribution and grazing. *Marine Ecology Progress Series* 201, 43–56.
- Boyd, P.W., Watson, A., Law, C.S., Abraham, E.R., et al., 2000. A mesoscale phytoplankton bloom in the polar Southern Ocean stimulated by iron fertilization. *Nature* 407, 695–702.
- Boyé, M., et al., 2002. Colloidal Fe accounts for a significant part of dissolved organic Fe complexes in the Southern Ocean. *EOS Transactions* 83 (4), 102.
- Bruland, K.W., Franks, R.P., Knauer, G., Martin, J.H., 1979. Sampling and analytical methods for the determination of copper, cadmium, zinc, and nickel in seawater. *Analytica Chimica Acta* 105, 233–245.
- Bruland, K.W., Rue, E.L., Smith, G.J., 2001. Iron and macronutrients in California coastal upwelling regimes: implications for diatom blooms. *Limnology and Oceanography* 46, 1661–1674.
- Buesseler, K., et al., 1996. An intercomparison of cross-flow filtration techniques for sampling marine colloids: overview and organic carbon results. *Marine Chemistry* 51, 1–31.
- Buffle, J., Perret, D., Newman, M., 1992. The use of filtration and ultrafiltration for size fractionation of aquatic particles, colloids and macromolecules. In: Buffle, J., Leeuwen, H.P.V. (Eds.), *Environmental Particles. IUPAC Series on Environmental Analytical and Physical Chemistry*. Lewis Publishers, Chelsea, MI, pp. 171–230.
- Cavender-Barnes, K.K., Mann, E.L., Chisholm, S.W., Ondrusek, M.E., Bidigare, R.R., 1999. Differential response of equatorial Pacific phytoplankton to iron fertilization. *Limnology and Oceanography* 44, 237–246.
- Chin, W.-C., Orellana, M.V., Verdugo, P., 1998. Spontaneous assembly of marine dissolved organic matter into polymer gels. *Nature* 391, 568–572.
- Coale, K.H., et al., 1996a. A massive phytoplankton bloom induced by an ecosystem-scale iron fertilization experiment in the equatorial Pacific. *Nature* 383, 495–501.

- Coale, K.H., Fitzwater, S.E., Gordon, R.M., Johnson, K.S., Barber, R.T., 1996b. Control of community growth and export production by upwelled iron in the equatorial Pacific Ocean. *Nature* 379, 621–624.
- Croot, P.L., et al., 2001. Retention of dissolved iron and Fe (II) in an iron induced Southern Ocean phytoplankton bloom. *Geophysical Research Letters* 28, 3425–3428.
- Dai, M.H., Martin, J.M., 1995. First data on the trace metal concentration level and behavior in two major Arctic River-estuarine systems (Ob and Yenisey) and in the adjacent Kara Sea. *Earth and Planetary Science Letters* 131, 127–141.
- Dai, M., et al., 1998. Evaluation of two cross-flow ultrafiltration membranes for isolating marine organic colloids. *Marine Chemistry* 62, 117–136.
- de Baar, H.J.M., de Jong, J.T.M., 2001. Distributions, sources and sinks of iron in seawater. In: Turner, D.R., Hunter, K.A. (Eds.), *The Biogeochemistry of Iron in Seawater*. Wiley, Chichester, pp. 123–253.
- Eppley, R.W., 1972. Temperature and phytoplankton growth in the sea. *Fisheries Bulletin* 70, 1063–1085.
- Erdner, D.L., Anderson, D.M., 1999. Ferredoxin and Flavodoxin as biochemical indicators of iron limitation during open ocean iron enrichment. *Limnology and Oceanography* 44 (7), 1609–1615.
- Gavis, J., 1976. Munk and Riley revisited: nutrient diffusion transport and rates of phytoplankton growth. *Journal of Marine Science* 34, 161–179.
- Gordon, R.M., Johnson, K.S., Coale, K.H., 1998. The behaviour of iron and other trace elements during Iron-Ex I and PlumEx experiments in the Equatorial Pacific. *Deep-Sea Research II* 45, 995–1041.
- Guieu, C., et al., 1998. On trace metal geochemistry in the Danube River and Western Black Sea. *Estuarine Coastal and Shelf Science* 47, 471–485.
- Guo, L., Wen, L.-S., Tang, D., Santschi, P.H., 2000. Re-examination of cross-flow ultrafiltration for sampling aquatic colloids: evidence from molecular probes. *Marine Chemistry* 69, 75–90.
- Gustafsson, Ö., Düker, A., Larsson, J., Andersson, P., Ingri, J., 2000. Functional separation of colloids and gravitoids in surface waters based on differential settling velocity: coupled cross-flow filtration-split flow-thin cell fractionation (CFF_SPLITT). *Limnology and Oceanography* 45, 1731–1742.
- Honeyman, B.D., Santschi, P.H., 1989. A Brownian-pumping model for trace metal scavenging: evidence from Th isotopes. *Journal of Marine Research* 47, 950–995.
- Hudson, R.J.M., Morel, F.M.M., 1993. Trace metal transport by marine microorganisms: implications of metal coordination kinetics. *Deep Sea Research* 40 (1), 129–150.
- Hutchins, D.A., Bruland, K.W., 1998. Iron-limited diatom growth and Si:N uptake ratios in a coastal upwelling regime. *Nature* 393, 561–564.
- Hutchins, D.A., Witter, A.E., Butler, A., Luther, G.W., 1999. Competition among marine phytoplankton for different chelated iron species. *Nature* 400, 858–860.
- Johnson, K.S., Coale, K.H., Elrod, V.A., Tindale, N.W., 1994. Iron photochemistry in waters from the equatorial Pacific. *Marine Chemistry* 46, 319–334.
- Kemp, A.E.S., Baldauf, J.G., 1993. Vast Neogene laminated diatom mat deposits from the eastern equatorial Pacific Ocean. *Nature* 362, 141–144.
- Landry, M.R., et al., 2000. Biological response to iron fertilization in the eastern equatorial Pacific (IronEx II). III. Dynamics of phytoplankton growth and microzooplankton grazing. *Marine Ecology Progress Series* 201, 57–72.
- Liu, X., Millero, F.J., 2002. The solubility of iron in seawater. *Marine Chemistry* 77 (1), 43–54.
- Maldonado, M.T., Boyd, P.W., LaRoche, J., Strzepek, A., et al., 2001. Iron uptake and physiological response of phytoplankton during a mesoscale Southern Ocean iron enrichment. *Limnology and Oceanography* 46, 1802–1808.
- Maranger, R., Bird, D.F., Price, N.M., 1998. Iron acquisition by photosynthetic marine phytoplankton from ingested bacteria. *Nature* 398, 248–251.
- Martin, J.H., 1990. Glacial-Interglacial CO₂ change: the iron hypothesis. *Paleoceanography* 5 (1), 1–13.
- Martin, J.H., Fitzwater, S.E., 1988. Iron deficiency limits phytoplankton growth in the north-east Pacific subarctic. *Nature* 331, 341–343.
- Martin, J.H., Gordon, R.M., 1988. Northeast Pacific iron distributions in relation to phytoplankton productivity. *Deep Sea Research* 35 (2), 177–196.
- Martin, J.H., et al., 1994. Testing the iron hypothesis in ecosystems of the equatorial Pacific Ocean. *Nature* 371, 123–129.
- Martin, J.M., Dai, M.H., Cauwet, G., 1995. Significance of colloids in the biogeochemical cycling of organic carbon and trace metals in the Venice Lagoon (Italy). *Limnology and Oceanography* 40, 119–131.
- Michaelis, M., Menten, M.L., 1913. Kinetics of invertase action. *Zeitschrift für Biochemie* 49, 333.
- Millero, F.J., Sotolongo, S., 1989. The oxidation of Fe (II) with H₂O₂ in seawater. *Geochimica et Cosmochimica Acta* 53, 1867–1873.
- Moffett, J.W., 2001. Transformations among different forms of iron in the ocean. In: Turner, D.R., Hunter, K.A. (Eds.), *The Biogeochemistry of Iron in Seawater*. John Wiley and Sons, Chichester, pp. 343–372.
- Nishioka, J., Takeda, S., Wong, C.S., Johnson, W.K., 2001. Size-fractionated iron concentrations in the northeast Pacific Ocean: distribution of soluble and small colloidal iron. *Marine Chemistry* 74, 157–179.
- Payne, J.W. (Ed.), 1980. *Microorganisms and Nitrogen Sources: Transport and Utilization of Amino Acids, Peptides, Proteins, and Related Substrates*. Wiley, New York.
- Pisias, N.G., Mayer, L.A., Mix, A.C., 1995. Paleocyanology of the eastern equatorial Pacific during the Neogene: synthesis of Leg 138 drilling results. *Proceedings of ODP, Scientific Results* 138, 5–24.
- Powell, R.T., Landing, W.M., Bauer, J.E., 1996. Colloidal trace metals, organic carbon and nitrogen in a southeastern US estuary. *Marine Chemistry* 55, 165–176.
- Rich, H.W., Morel, F.M.M., 1990. Availability of well-defined iron colloids to the marine diatom *Thalassiosira weissflogii*. *Limnology and Oceanography* 35, 652–662.
- Rue, E.L., Bruland, K.W., 1997. The role of organic complexation on ambient iron chemistry in the equatorial Pacific Ocean and

- the response of a mesoscale iron addition experiment. *Limnology and Oceanography* 42, 901–910.
- Sanudo-Wilhelmy, S.A., Rivera-Duarte, I., Flegal, A.R., 1996. Distribution of colloidal trace metals in the San Francisco Bay estuary. *Geochimica Cosmochimica Acta* 60, 4933–4944.
- Sigman, D.M., Boyle, E.A., 2000. Glacial/interglacial variations in atmospheric carbon dioxide. *Nature* 407, 859–869.
- Steinberg, P.A., Millero, F.J., Zhu, X.R., 1998. Carbonate system response to iron enrichment. *Marine Chemistry* 62, 31–43.
- Sunda, W.G., 2001. Bioavailability and bioaccumulation of iron in the sea. In: Turner, D.R., Hunter, K.A. (Eds.), *The Biogeochemistry of Iron in Seawater*. Wiley, Chichester, pp. 41–84.
- Sunda, W.G., Huntsman, S.A., 1995. Iron uptake and growth limitation in oceanic and coastal phytoplankton. *Marine Chemistry* 50 (1), 189–206.
- Sunda, W.G., Huntsman, S.A., 1998. Interrelated effects of iron, light and cell size on marine phytoplankton growth. *Nature* 390, 389–392.
- Takeda, S., 1998. Influence of iron availability on nutrient consumption ratio of diatoms in oceanic waters. *Nature* 393, 774–777.
- Takeda, S., et al., 2002. Biogeochemical Processes During the Subarctic Pacific Iron Experiment for Ecosystem Dynamics Study (SEEDS). Ocean Sciences Meeting, Honolulu, HI.
- Timmermans, L.R., et al., 2001. Growth rates of large and small Southern Ocean diatoms in relation to availability of iron in natural seawater. *Limnology and Oceanography* 46 (2), 260–266.
- Völker, C., Wolf-Gladrow, D.A., 1999. Physical limits on iron uptake mediated by siderophores or surface reductases. *Marine Chemistry* 65, 227–244.
- Waite, T.D., 2001. Thermodynamics of the iron system in seawater. In: Turner, D.R., Hunter, K.A. (Eds.), *The Biogeochemistry of Iron in Seawater*. Wiley, Chichester, pp. 291–342.
- Wells, M.L., 2002. Marine colloids and trace metals. In: Hansell, D., Carlson, C. (Eds.), *The Biogeochemistry of Marine Dissolved Organic Matter*. Academic Press, San Diego, USA.
- Wells, M.L., Bruland, K.W., 1998. An improved method for rapid preconcentration and determination of bioactive trace metals in seawater using solid phase extraction and high resolution inductively coupled plasma mass spectrometry. *Marine Chemistry* 63 (1–2), 145–153.
- Wells, M.L., Zorkin, N.G., Lewis, A.G., 1983. The role of colloid chemistry in providing a source of iron to phytoplankton. *Journal of Marine Research* 41, 731–746.
- Wells, M.L., Mayer, L.M., Donard, O.F.X., de Souza Sierra, M.M., Ackleson, S., 1991a. The photolysis of colloidal iron in the oceans. *Nature* 353, 248–250.
- Wells, M.L., Mayer, L.M., Guillard, R.R.L., 1991b. A chemical method for estimating the availability of iron to phytoplankton in seawater. *Marine Chemistry* 33, 23–40.
- Wells, M.L., Price, N.M., Bruland, K.W., 1995. Iron chemistry in seawater and its relationship to phytoplankton: a progress report. *Marine Chemistry* 48, 157–182.
- Wells, M.L., Vallis, G., Silver, E., 1999. Tectonic Processes in Papua New Guinea and Paleo Diatom Blooms in the Eastern Equatorial Pacific. *Nature* 398, 601–604.
- Wells, M.L., Smith, G.J., Bruland, K.W., 2000. The distribution of colloidal and particulate bioactive metals in Narragansett Bay, RI. *Marine Chemistry* 71, 143–163.
- Wen, L.S., Santschi, P., Gill, G., Paternostro, C., 1999. Estuarine Trace metal distributions in Galveston Bay: importance of colloidal forms in the speciation of the dissolved phase. *Marine Chemistry* 63, 185–212.
- Whitehouse, B.G., Yeats, P.A., Strain, P.M., 1990. Cross-flow filtration of colloids from aquatic environments. *Limnology and Oceanography* 25, 1368–1375.
- Wu, J.-F., Boyle, E., Sunda, W., Wu, L.-S., 2001. Soluble and colloidal iron in the oligotrophic North Atlantic and North Pacific. *Science of the Total Environment* 293, 847–849.